Three-dimensional observation system for pellet ablation traveling in the high-temperature plasmas

Ryuichi Sakamoto[a] and Hiroshi Yamada
National Institute for Fusion Science, Toki, Gifu 509-5292, Japan

(Received 21 June 2005; accepted 7 September 2005; published online 10 October 2005)

In order to investigate the ablation of a solid hydrogen pellet, which is injected into a high-temperature plasma with high speed (~1 km/s) for the plasma refueling, a three-dimensional observation system using a fast camera has been developed. A stereo method has been employed to obtain the three-dimensional information of the pellet ablation. A pair of the stereo images, which have been taken from different locations, has been focused onto a single fast camera by using a bifurcated fiber scope to ensure the simultaneity of both images. The projection matrix, which is used for stereo reconstruction, is calibrated by taking images of a model plane of known coordinates from the actual camera positions. The measuring error of the stereo observation is within 2% in the depth direction. © *2005 American Institute of Physics.* [DOI: 10.1063/1.2093770]

I. INTRODUCTION

Pellet injection has a potential for high-efficiency fueling in a magnetically confined high-temperature plasma since it can supply the hydrogen directly to the core plasma. Pellet injection, therefore, is one of the promising candidates for plasma refueling in a future fusion reactor. In fact, pellet injection has extended the operational regime to higher densities while maintaining favorable confinement properties.[1,2] On the other hand, obvious degradation of the fueling efficiency is observed in high-temperature plasmas under high-power heating conditions.[3] The fact that the pellet mass-deposition profile is skewed toward the edge when compared to the measured pellet penetration depth[2,4] and the pellet ablatant promptly drifts towards the low-magnetic-field direction,[5,6] have been confirmed in several experiments. These phenomena suggest that the behavior of the pellet ablatant can be a critical issue in considering the fueling efficiency. In order to optimize the pellet fueling based on an understanding of the mechanism, it is important to investigate the pellet ablation and subsequent drift of the ablatant. For this purpose, three-dimensional observation with a high sampling rate is needed since the pellet ablation related phenomena are relatively short (typically less than 10^{-3} s) and the spatial structure of the pellet ablatant changes continuously while moving, which is caused by interaction with the plasma and the confining magnetic field in addition to the initial injection inertia. In particular, a three-dimensional observation is needed in the case of helical systems such as the large helical device (LHD), because the interaction between the pellet ablatant and the magnetic field is complicated due to the three-dimensional characteristic of the confining magnetic field.[7] Many pellet ablation studies have been made; however, a fast and accurate three-dimensional measurement has not been established yet.

If there is no limitation on observation positions, a three-dimensional tomographic reconstruction[8] is a powerful method for obtaining three-dimensional information; however, the observation positions and their available numbers are considerably restricted in plasma experiment devices. In this study, therefore, we have employed stereoscopic measurement, which uses only a pair of observation points, to get three-dimensional information from two-dimensional observations. The stereoscopic analysis is a method to estimate the three-dimensional information from the discrepancy of two (multiple) images, which are taken from different locations. The camera calibration has been carried out to minimize the error due to lens distortion, image digitalization, etc.

II. DIAGNOSTIC SYSTEM

A. Stereoscopic analysis principle

A three-dimensional spatial point, which is denoted by $\mathbf{M}=[X,Y,Z]^T$, should be projected to a two-dimensional image point, which is denoted by $\mathbf{m}=[u,v]^T$, on an image. Assuming a pinhole camera model, the relationship between $\mathbf{M}$ and $\mathbf{m}$ is given by

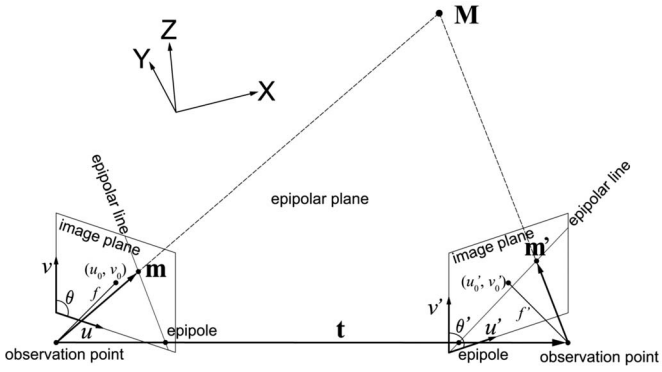

FIG. 1. Measurement principle of the stereo observation.

[a]Electronic mail: sakamoto@LHD.nifs.ac.jp

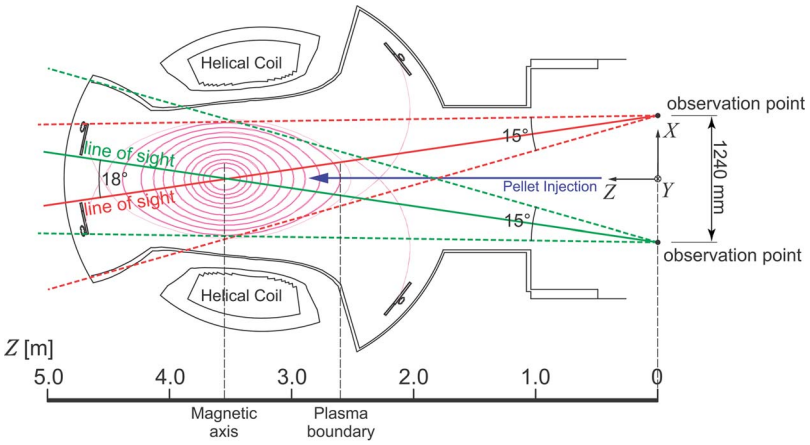

FIG. 2. Pellet injection location and the stereo observation points on LHD. The Z axis is defined as the pellet injection direction and its coordinate value is indicated in meters. A pellet enters the plasma at $Z=2.6$ m.

$$s\tilde{\mathbf{m}} = \mathbf{P}\tilde{\mathbf{M}}, \tag{1}$$

where s is an arbitrary scale factor and $\mathbf{P}$ is a projection matrix. The projection matrix is composed of extrinsic parameters $[\mathbf{R},\mathbf{t}]$, which relate the three-dimensional coordinate system and the two-dimensional image coordinate system with a rotational matrix $\mathbf{R}$ and a translational vector $\mathbf{t}$, and an intrinsic parameter $\mathbf{A}$, which consists of the geometric and optical characteristics of the camera. Namely, the projection matrix is given by

$$\mathbf{P} = \mathbf{A}[\mathbf{R},\mathbf{t}] = \begin{bmatrix} fk_u & -fk_u \cot\theta & u_0 \\ 0 & fk_v/\sin\theta & v_0 \\ 0 & 0 & 1 \end{bmatrix} \begin{bmatrix} R_{11} & R_{12} & R_{13} & t_X \\ R_{21} & R_{22} & R_{23} & t_Y \\ R_{31} & R_{32} & R_{33} & t_Z \end{bmatrix} = \begin{bmatrix} P_{11} & P_{12} & P_{13} & P_{14} \\ P_{21} & P_{22} & P_{23} & P_{24} \\ P_{31} & P_{32} & P_{33} & P_{34} \end{bmatrix},$$

where f is the focal length, k_u and k_v are scale factors in the image u and v axes, (u_0,v_0) are the coordinates of the principal point, and θ is the angle of the two image axes. If two cameras, which are located at different positions as shown in Fig. 1, are employed, the three-dimensional point $\mathbf{M}$ is projected to each image coordinate $\mathbf{m},\mathbf{m}'$ by the projection matrix for each camera $\mathbf{P},\mathbf{P}'$, and the following expression is derived from the $s\tilde{\mathbf{m}}=\mathbf{P}\tilde{\mathbf{M}}$ and $s'\tilde{\mathbf{m}}'=\mathbf{P}'\tilde{\mathbf{M}}$:

$$\begin{bmatrix} P_{14}-uP_{34} \\ P_{24}-vP_{34} \\ P'_{14}-u'P'_{34} \\ P'_{24}-v'P'_{34} \end{bmatrix} = \begin{bmatrix} uP_{31}-P_{11} & uP_{32}-P_{12} & uP_{33}-P_{13} \\ vP_{31}-P_{21} & vP_{32}-P_{22} & vP_{33}-P_{23} \\ u'P'_{31}-P'_{11} & u'P'_{32}-P'_{12} & u'P'_{33}-P'_{13} \\ v'P'_{31}-P'_{21} & v'P'_{32}-P'_{22} & v'P'_{33}-P'_{23} \end{bmatrix} \times \begin{bmatrix} X \\ Y \\ Z \end{bmatrix}. \tag{2}$$

If the projection matrices are known, the coordinates of the spatial points are obtained from the corresponding coordinates of each image. Because the spatial point $\mathbf{M}$ and the image points $\mathbf{m},\mathbf{m}'$ should exist in the same plane (epipolar plane), if a certain point in one image is given, the corresponding point in the other image is confined to the epipolar line, which is the intersection line of the image plane and the epipolar plane. In order to make it easy to search the corresponding points, a pair of stereo images are rectified by homography matrices to virtually parallel stereo images in which the line of sights are parallel and epipolar lines are parallel with the horizontal axis.

B. Experimental setup

Figure 2 shows a horizontally elongated poloidal cross section of the LHD,[9] which is the world's largest helical magnetic plasma-confinement device with a major radius of 3.9 m and an average minor radius of 0.6 m. The pellet injection location is on the midplane from the outboard side as shown by the arrow. The motion of the pellet ablation emission is observed from two positions, namely, above and below the injection port as shown by the dashed lines. The observation positions are separated by 1240 mm and the angle between two lines of sight is 18°.

Because the lifetime of the pellet in a high-temperature plasma is within a couple of 10^{-3} s in most cases, a fast camera (Vision Research, Inc. Phantom v7), which is equipped with a 12 bit self-resetting complementary metal-oxide semiconductor (SR-CMOS) sensor, has been employed to observe the temporal behavior. The frame rate of the camera is 20 kHz for 464×192 pixels and the exposure time is 2–48 μs. A pair of the stereo images, which are taken from different locations, has been focused onto the single fast camera's focal plane array of SR-CMOS sensors by using a bifurcated fiber scope to ensure the simultaneity of both images. Figure 3(a) shows the bifurcated fiber scope, which consists of a pair of 50 000 element quartz fiber scopes with a stainless-steel flexible protective tube. The overall length is 15 m and the bifurcated portions are about 5 m in length. Each bifurcated end has an objective lens, which has a field of view of 15°. The bundled end has an imaging lens, which can project a pair of images onto the imaging sensor as shown Fig. 3(b), with the lens mounted to the camera.

C. Camera calibration

The projection matrix is estimated by taking images of a model plane of known coordinates from the actual camera

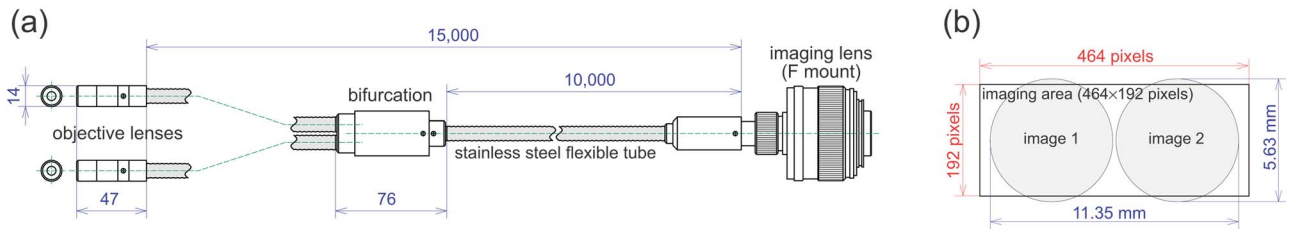

FIG. 3. Schematic drawing of (a) the bifurcated fiber scope and (b) its imaging area on the sensor of the fast camera. Measurements are given in mm.

positions. Here we take the origin of the spatial coordinates as the midpoint between the observation points, and the Z axis is defined as the pellet injection direction as shown in Fig. 2.

The following relations are derived from Eq. (1) by substituting the three-dimensional coordinates of a spatial point $[X_i, Y_i, Z_i]$ and the two-dimensional coordinates of the projected image point $[u_i, v_i]$:

$$\begin{cases} X_iP_{11} + Y_iP_{12} + Z_iP_{13} + P_{14} - u_iX_iP_{31} - u_iY_iP_{32} - u_iZ_iP_{33} - u_iP_{34} = 0, \\ X_iP_{21} + Y_iP_{22} + Z_iP_{23} + P_{24} - v_iX_iP_{31} - v_iY_iP_{32} - v_iZ_iP_{33} - v_iP_{34} = 0. \end{cases} \tag{3}$$

Since the projection matrices have 12 elements, at least six pairs of the points are required to estimate the projection matrix. If we have n pairs of the points, by stacking n such equations as in Eq. (3) we get

$$\mathbf{Ap} = \mathbf{0}, \tag{4}$$

with

$$\mathbf{A} = \begin{bmatrix} X_1 & Y_1 & Z_1 & 1 & 0 & 0 & 0 & 0 & -u_1X_1 & -u_1Y_1 & -u_1Z_1 & u_1 \\ 0 & 0 & 0 & 0 & X_1 & Y_1 & Z_1 & 1 & -v_1X_1 & -v_1Y_1 & -v_1Z_1 & v_1 \\ \vdots & \vdots & \vdots & \vdots & \vdots & \vdots & \vdots & \vdots & \vdots & \vdots & \vdots & \vdots \\ X_n & Y_n & Z_n & 1 & 0 & 0 & 0 & 0 & -u_nX_n & -u_nY_n & -u_nZ_n & u_n \\ 0 & 0 & 0 & 0 & X_n & Y_n & Z_n & 1 & -v_nX_n & -v_nY_n & -v_nZ_n & v_n \end{bmatrix},$$

$$\mathbf{p} = [P_{11}, P_{12}, P_{13}, P_{14}, P_{21}, P_{22}, P_{23}, P_{24}, P_{31}, P_{32}, P_{33}, P_{34}]^T.$$

The solution of Eq. (4) is given as the eigenvector of $\mathbf{A}^T\mathbf{A}$ associated with the smallest eigenvalue.

The model plane contains a 6×6 regular-interval dot pattern, so there are 36 points. The interval of the dots is 50 mm. The central nominal vector of the model plane is set parallel to the Z axis and the distance from the origin is changed in 50 mm interval in the range of 2.3–3.0 m. Therefore a total of $36 \times 14 = 504$ spatial points were used for the estimation of the projection matrix.

III. EXPERIMENTAL RESULT AND DISCUSSION

A. Measuring accuracy

The accuracy of the stereoscopic measurement is examined with the model plane, which was used in the camera calibration. Figure 4 shows the measuring accuracy of the Z axis, namely, the depth direction. The horizontal axis and vertical axis indicate the actual Z value of the model plane and the stereo-reconstructed Z value, respectively. The stereo-reconstructed Z value shows good agreement with the actual Z value within the range of the error. The thick error bars indicate the maximum and minimum stereo-reconstructed Z value for a model plane, which is put at Z. The Z error is about ±30 mm, that is, ±2% for the Z coordinate as shown by thin alternate long and short dash lines. The thin error bars indicate the range of scatter in the reconstruction when the stereo matching has a ±3 pixel error. Figure 5

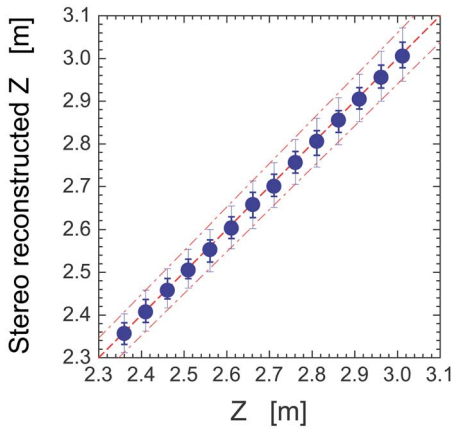

FIG. 4. Stereo-reconstructed Z coordinate value actual position of the model plane. Thin alternate long and short dash lines indicate ±2% error.

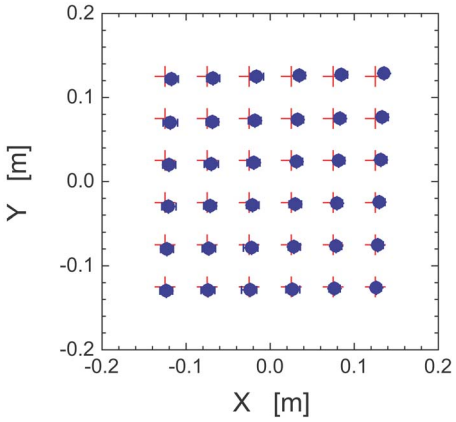

FIG. 5. Stereo-reconstructed accuracy in the *X*-*Y* plane. The cross symbol indicates actual points on the model plane. The closed circles indicate the average of the *X*-*Y* data in the different *Z* coordinates.

shows the measuring accuracy of the *X*-*Y* plane. The cross symbol indicates actual points of the 6×6 regular-interval dot pattern. The stereo-reconstructed points are indicated by the closed circles with error bars. Several stereo-reconstructed points deviate from the actual points, but the error is sufficiently small, i.e., the maximum error in the *X* and *Y* directions is 10 and 5 mm, respectively. It is confirmed that the stereo reconstruction provides a good estimation of the spatial coordinates with linearity.

B. Observation of the pellet ablatant

In order to demonstrate the usefulness of this measurement, the ablation behavior of a pellet, which is injected into the LHD plasmas, has been analyzed. Figure 6 shows the temporal change of the pellet ablation light intensity, which is measured by a photodiode with a H_α filter. Assuming that the initial pellet velocity is maintained during the ablation, the pellet position can be predicted as a broken line in Fig. 6. The stereo observation has been carried out with a sampling rate of 20 000 images per second and an exposure time of 4 μs. In this experiment, the lifetime of the pellet is relatively long (>3 ms) because of the low-temperature target plasma (T_e=0.7 keV) and about 70 pairs of stereo images are obtained during the ablation. Figure 7(a) shows the stereo pair of the typical pellet ablatant. An epipolar line is parallel to the horizontal axis in both images. The emission intensity distribution along the epipolar lines is shown in Fig. 7(b). Stereo matching has been carried out by a feature-based stereo-matching procedure, i.e., the corresponding points in each image are defined by the brightest points along the epipolar lines. The pellet position, which is measured by the stereo observation, is plotted in Fig. 6 by open circles. The pellet position, which is reconstructed by stereo analysis, showed good agreement with the predicted pellet position. In other words, it has been confirmed by this method that the initial velocity of the pellet is maintained during ablation in a hot plasma. At the same time, we can observe the structure of the ablating pellet on the *X*-*Y* plane using the images.

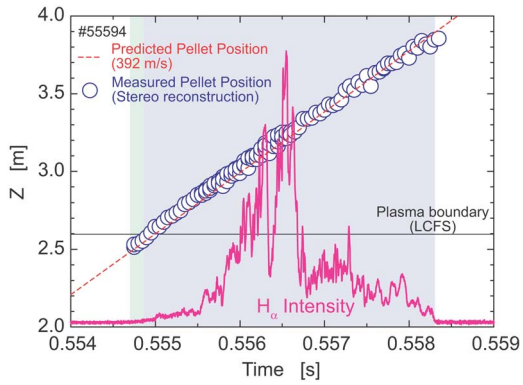

FIG. 6. Temporal change of the predicted and stereo-reconstructed pellet position and H_α intensity.

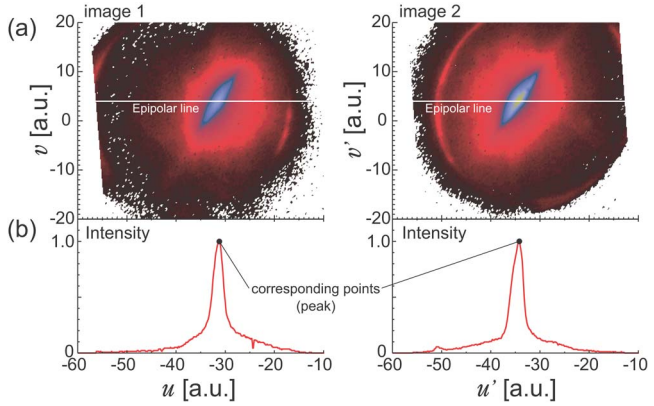

FIG. 7. (a) Typical stereo pair of the ablating pellet and (b) the emission intensity distribution along the epipolar lines.

We developed the ability to obtain three-dimensional information of the obvious corresponding points such as emission peak. With respect to the subjects for further study, a full three-dimensional reconstruction using an area-based stereo-matching procedure is required to perform a more detailed observation. In addition, multipoint simultaneous observation is also useful for reducing the blind spot and performing stable stereo analysis.

[1] S. L. Milora, Nucl. Fusion **35**, 657 (1995).
[2] R. Sakamoto *et al.*, Nucl. Fusion **41**, 381 (2001).
[3] P. T. Lang *et al.*, Nucl. Fusion **43**, 1674 (2003).
[4] L. R. Baylor, T. C. Jernigan, and C. Hsieh, Fusion Technol. **34**, 425 (1998).
[5] H. W. Müller *et al.*, Phys. Rev. Lett. **83**, 2199 (1999).
[6] J. de Kloe, E. Noordermeer, N. J. Lopes Cardozo, and A. A. M. Oomens, Phys. Rev. Lett. **82**, 2685 (1999).
[7] R. Sakamoto *et al.*, *29th European Physical Society Conference on Plasma Physics and Controlled Fusion, 17–21 June 2002, Montreux, Switzerland* (European Physical Society, 2002), ECA 26B, P-1.074.
[8] A. C. Kak and M. Slaney, *Principles of Computerized Tomographic Imaging: Classics in Applied Mathematics* 33 (Society for Industrial and Applied Mathematics, Philadelphia, 2001).
[9] O. Motojima *et al.*, Nucl. Fusion **43**, 1674 (2003).